CrossMark

Mechanical and Tribological Behavior of Microcrystalline CVD Diamond Coatings

Sajad Hussain Din[1] · N. A. Sheikh[1] · M. Mursaleen Butt[1]

Abstract

Smooth and adhesive microcrystalline CVD diamond coatings have been acquired successfully on chemically etched titanium alloy (Ti6Al4V) substrates, using hot filament chemical vapor deposition technique. The mechanical and tribological characteristics of HFCVD microcrystalline diamond coatings on titanium alloy (Ti6Al4V) substrates are investigated in this research. SEM and Raman spectroscopy were used to study the morphology and quality of the coatings. The surface roughness has been determined by 3d profilometer measurements. A ball-on-disk tribometer was used to characterize the friction and wear of the coatings. The frictional behavior of the MCD coating was studied, when sliding against smooth alumina ball with increasing load (1–10 N). A coefficient of friction of ~ 0.3–0.287 was obtained at a sliding speed of 12 m/s. The wear of the diamond coating is negligible. The alumina balls are worn out quickly as compared to the diamond coatings. Nanoindentation tests were carried out using Berkovich nanoindenter, and the average super-hardness of MCD coatings was found to be 55 GPa.

1 Introduction

From the beginning of its invention, diamond has drawn a great attention of the research community [1]. Diamond has great promising applications due to its unique mechanical, thermal, electrical and optical properties [2]. Chemical vapor deposition (CVD) method can be used to synthesize diamond in thin film form, at suitable conditions [3, 4]. Growth of thin solid films on the substrates through diffusion can be achieved by CVD process which involves the gas-phase homogeneous and heterogeneous chemical reactions [5]. The precursor gases inside the CVD chamber can be actuated with the help of heat (thermal CVD), high-frequency radiation (photo-assisted CVD) or by using plasma (plasma-enhanced CVD) [6]. Hot filament chemical vapor deposition (HFCVD) reactors can be used for large-area depositions and uniform coatings on complex shaped tools. The activation energy for the precursor gases can be achieved through thermal energy generated by the resistive heating of

refractory filaments [7]. The commonly used precursor gases for the growth of diamond are methane (CH_4) and hydrogen (H_2) [8]. To stabilize the diamond lattice and for etching the graphite nuclei during the growth process, hydrogen plays an important role in controlling the quality of diamond growth and methane is the source gas for carbon [9]. Methane concentration is the key growth parameter, which controls the crystallinity and grain size of the diamond coating [10]. It generally varies from 0.5 to 10%. The growth parameters that also contribute to the grain size, quality and growth rate of the diamond coatings are substrate to filament distance, substrate temperature and filament temperature and chamber pressure [11]. A small quantity of hydrocarbon gas (CH_4, C_2H_2, etc.) in excess hydrogen (H_2) is the requirement in deposition of diamond coatings using a CVD process which involves the gas-phase decomposition of precursor gases [12]. The deposition conditions such as temperature and pressure, substrate properties and deposition time, and a typical gas mixture of 1% CH_4 in H_2 produce highly crystalline diamond films with grain sizes in the micron range [13]. Hot filament provides required energy for the dissociation of the precursor gases to form the radical species. These gas species will go through set of complex reactions, after

✉ Sajad Hussain Din
   sajad_08phd12@nitsri.net

[1] Department of Mechanical Engineering, National Institute of Technology Srinagar, Srinagar, 190006, India

passing through the activation region, and move toward the substrate which is at high temperature (700–900 °C) [14].

The metal filament (such as W, Ta or Re) is heated up to approximately 2200 °C to dissociate the precursor gases [15]. Chamber pressure and flow rates are controlled by throttle valve and mass flow controllers, respectively [16]. Crystalline and faceted surface morphology has been found to be exhibited by the diamond coating with low methane concentration (2%), whereas that with high methane concentration result in smooth surface. May et al. studied the effect of methane concentration on the diamond crystallite size. It was found that the grain size of the film decreases to the order of hundreds down to tens of nanometers, by increasing the methane in the CH_4/H_2 gas mixture from 1 to 5%. Such diamond coatings with the grain size of few nanometers are smoother than the conventional MCD coatings. Liang et al. studied the effect of chamber pressure on the grain size of diamond coatings. A gradual reduction in the diamond grain size was detected from sub-micrometer to nanometer scale with the decreasing growth pressure from 37.5 to 1 Torr. Grain size of the CVD diamond coatings is maintained by the process parameters such as gas mixture, process pressure and substrate temperature [17–19]. In a typical CH_4/H_2 system for the growth of diamond, 1% of methane concentration favors the columnar grain growth and yields phase pure MCD (grain size > 500 nm) [20, 21].

In the present study, smooth and adhesive (3 μm thick) microcrystalline diamond coatings have been successfully achieved on titanium alloy (Ti6Al4V) substrates using HFCVD technique. The analysis revealed the high-phase-purity, well-oriented crystalline and columnar growth of the coatings. The friction characteristics of the diamond-coated titanium alloy substrates were compared with uncoated one, using ball-on-disk-type linear reciprocating micro-tribometer, sliding against smooth alumina (Al_2O_3) ceramic ball under dry sliding conditions.

2 Experimental Details

In order to realize adhesive and continuous diamond coatings on titanium alloy (Ti6Al4V) substrates, surface pre-treatment is an important step. The stepwise surface pre-treatment procedure mainly involves: (1) cleaning the substrate with organic solvents, (2) chemical etching of titanium alloy and (3) nano-diamond seeding. Mechanical interlocking is the main mechanism of adhesion between the CVD diamond and titanium alloy substrate. Good interfacial adhesion can be attained by providing the complicated cavities on the titanium alloy substrate. To produce intricate cavities, chemical etching is the extensively followed surface pre-treatment process. To attain high nucleation densities, nanodiamond seeding is the final step of surface pre-treatment for diamond growth process.

Diamond can grow directly on the chemically etched titanium substrates, but may end up with porous non-uniform island growth. In order to grow thin pin-hole-free coalesced and uniform film with small grains, a high nucleation density is required [22]. There are various methods to increase the nucleation density such as micro-scratching, mechanical scratching using micron-sized diamond particles, nanodiamond seeding by ultrasonic agitation and bias-enhanced nucleation by ion bombardment [23]. The nanodiamond particles adhere to the substrate by van der Waals interactions and turn out as nucleation centers, by treating the substrate with ultrasonication in nanodiamond suspension [24]. To achieve nucleation densities as high as 10^{11} nuclei/cm^2, nanodiamond seeding is the most promising technique. Such high nucleation densities can assist in the formation of thin and uniform coatings [25]. Titanium alloy substrates of size 2.3 cm diameter and thickness 0.3 cm, with surface roughness (Ra) of ~0.35 μm, were cleaned in ethyl alcohol with ultrasonic agitation to eliminate the impurities from the surface. MCD CVD diamond coatings were successfully deposited on these substrates, using HFCVD technique with approximately uniform thickness of ~3 μm. Structural characteristics of these coatings were studied using grazing incidence X-ray diffraction (PANalytical) technique with Cu Kα ($\lambda = 0.154$ nm) radiation at 3° grazing angle and confocal Raman microscope (Alpha 300R, WITec) at an excitation wavelength of 532 nm. Surface morphology of these coatings was studied using a high-resolution scanning electron microscope (HRSEM, Quanta 3D, FEI). Nanoindentation tests were done using triboindenter (TI 950, HYSITRON) with a Berkovich tip of total included angle ($2a$) = 130.5°, radius of curvature approximately 150 nm and at a 10 mN trapezoidal load cycle. The values of hardness (H) were measured from the load–displacement data. The values of elastic modulus (E) were calculated using Oliver and Pharr mathematical procedure. Friction characteristics were carried out using a ball-on-disk-type linear reciprocating micro-tribometer (CSM Instruments, Switzerland) under dry sliding conditions. Alumina (Al_2O_3) ball of size 6 mm was used as sliding ball, applying at three different normal loads of 1, 5 and 10 N. A sliding speed of 12 cm/s, frequency of 8 Hz and a friction stroke length of 10 mm were used for the total sliding distance of 200 m. Table 1 shows the coating experiment carried out to establish the growth parameters for depositing MCD coatings.

Table 1 Growth parameters for depositing MCD coatings

Coating type	%[CH_4/H_2]	Pressure (Torr)	Time (h)
MCD	2	36	3

3 Microstructural Characterization and Tribological Properties

Surface topography and cross-sectional morphology of the MCD coatings were mainly characterized using scanning electron microscopy (SEM) technique. Also, SEM was used to study the wear track morphologies. Microcrystalline features of the diamond coatings were imaged with 3d profilometer. Energy-dispersive spectroscopy (EDS) detector attached to the scanning electron microscope was used for the elemental analysis of the work materials and wear tracks. Structural characteristics of the diamond coatings were characterized using XRD technique and Raman spectroscopy.

3.1 Scanning Electron Microscopy

Figure 1a shows the structure of substrate titanium alloy without CVD coating, and Fig. 1b shows the compositional analysis of the substrate. Figure 1c shows the structure of microcrystalline diamond coatings, and Fig. 1d shows its compositional analysis. Scanning electron microscope coupled with energy-dispersive spectroscopy (EDS) attachment is the most useful tool to study the surface morphology and composition of the near-surface regions of the specimen. EDS is an analytical technique mainly used to study the chemical composition of the surface. Columnar structure of grains and faceted structure was exhibited by MCD coatings. Generally, well-crystallized MCD films exhibit good adhesion to ceramic substrates. From SEM micrographs, it can be observed that MCD coatings are crack free, continuous, compact and able to act as protective coatings. It is obvious that the grain size is 200 nm to 1 μm. Generally, the thicker the film is, the larger the grain size is and rougher the surface of the diamond coatings in MCD is.

3.2 Raman Spectroscopy

Raman spectroscopy is a nondestructive and powerful technique to evaluate the quality of the diamond coatings (the presence of non-diamond carbon phases). When the monochromatic radiation (light) is incident on the matter, this light may be absorbed, reflected or scattered due to interaction. Light scattered from the matter may have one (Rayleigh
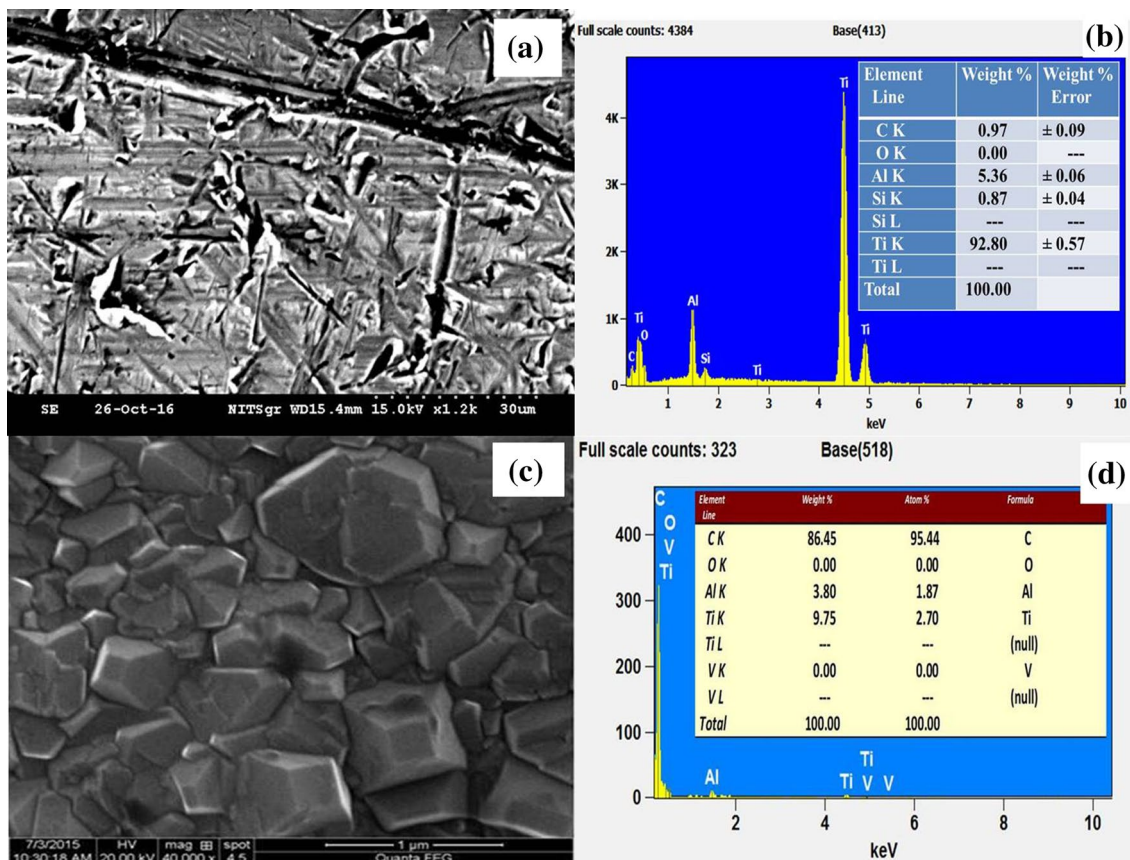

Fig. 1 a SEM image displaying morphology of the substrate without diamond coating. **b** EDS analysis of substrate. **c** SEM image displaying morphology of the diamond coating. **d** EDS analysis of diamond coatings

scattering) or more (Stokes and anti-Stokes Raman scattering) scattering events. The scattering event that occurs without a change in the wavelength is called Rayleigh scattering. A change in the wavelength of the light is called Raman scattering, which is a fingerprint characteristic for the type of the molecules that are involved in the scattering process. After the Raman scattering, photons may have either higher or lower energy, depending on the vibrational state of that particular molecule [26]. Spectral information with high resolution of 1 cm^{-1} was acquired using a $20 \times$ objective and 1800/mm grating at an excitation wavelength of 532 nm.

Raman spectroscopy is the widely used structural characterization technique to study the crystallinity of diamond and related materials. It is a fingerprint characterization technique to distinguish between the different allotropes of carbon and even between the diamond coatings of different crystallinity because of its ability to distinguish between the vibrational modes of sp^3 and sp^2 bonding configurations. However, care should be taken while interpreting the Raman spectra of diamond coatings because Raman scattering is about 50 times more sensitive to π-bonded amorphous carbon and graphite than to the phonon band of diamond. Diamond belongs to the FCC lattice with motif 2 and space group Fd-3 m. Highly crystalline and phase pure cubic diamond has a single Raman-active first-order phonon mode at the center of the Brillouin zone, and this first-order band appears at 1332 cm^{-1} as a single sharp line. Small shift in the band wave number can be related to the stress state of the deposited films, while the right shift indicates compressive stress and the left shift indicates tensile stress [27, 28]. Figure 2 shows the Raman spectra of MCD coatings. The residual tensile stresses for the MCD diamond coating system can be calculated as $-0.348\,(1333{-}1332) = -0.348\,\text{GPa}$, where negative sign implies compressive stress.
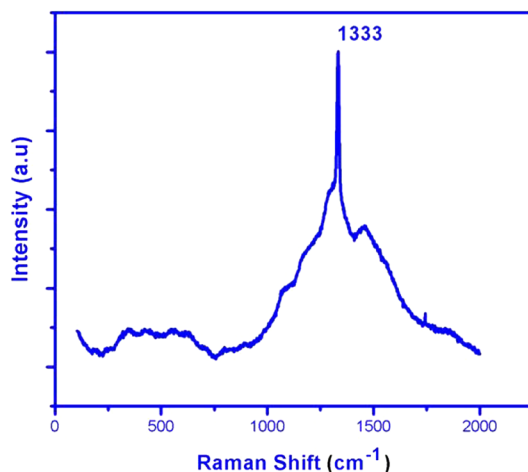

Fig. 2 Typical Raman spectra of the titanium alloy samples coated with CVD diamond

3.3 3d Profilometer Analysis

Figure 3a–c shows the 3d profilometer images of substrate. The 3d profilometer imaging was carried out, and the 3d height image gives better topographical contrast and details in comparison with HRSEM image. Figure 1c shows the surface topography of the MCD coating obtained using HRSEM. However, individual micro-sized grains of the MCD coating cannot be probed using scanning electron microscopy due to charging problem. Similar area of the MCD coating was probed using 3d profilometer and is presented in Fig. 3d–f; it shows the 3d profilometer height image of the MCD coatings at a scanning areas of $3.5 \times 4.4\ \mu\text{m}^2$. Ballas type smooth grains that were observed on the MCD surface are having considerable micro-tribological significance. Height details of the features were represented as a color scale on the right side of the 3d profilometer height image.

Height imaging and phase imaging are the two important variations of the tapping mode. Height image gives the topographical information, whereas phase imaging is the mapping of the phase difference between the driver signal and the oscillations of the cantilever (i.e., response signal). Phase shifts are recorded as bright and dark regions, comparable to the way that the topographical changes are indicated in height image. Sectioning is an important function in the post-processing of the captured image. Height, depth and width measurements can be easily taken using this function by deriving the vertical profile of the surface along the sectioning line.

3.4 Structural Characterization Methods

X-ray diffraction (XRD) is an exceptional technique to recognize and study the structural characteristics of the crystalline materials, and it offers unmatched accuracy in the quantification of atomic spacing. Crystallinity of the diamond coatings was studied using XRD instrument with Cu Kα ($\lambda = 0.15{,}405$ nm) radiation. The measurements were taken in glancing incidence mode (GIXRD) at 3° glancing angle, where detector scans in the vertical plane. Figure 4 shows the XRD analysis of the coatings. A typical XRD pattern of the polycrystalline diamond coating shows diffraction peaks corresponding to (111) and (220) planes at the diffraction angle (2θ) of 43.9° and 75.4°, respectively. Majority of the crystallites in medium-grained/microcrystalline diamond coatings are oriented in the <111> direction.

3.5 Mechanical Aspects of CVD Diamond

The mechanical properties such as hardness and elastic modulus of the material can be obtained directly from the indentation load and load–displacement measurements. Usually,
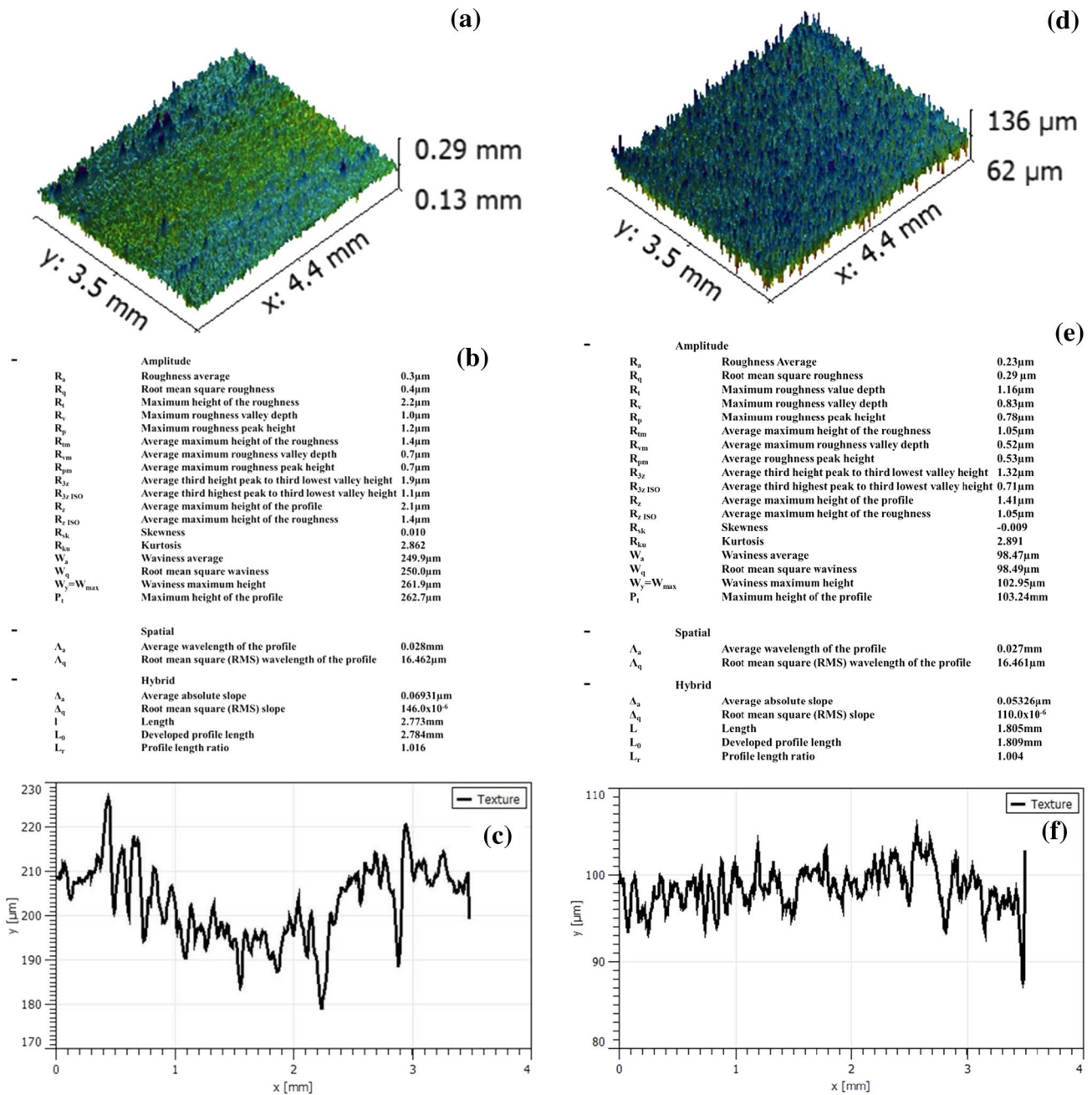
(a)

(d)

(b)

Amplitude		
R_a	Roughness average	0.3μm
R_q	Root mean square roughness	0.4μm
R_t	Maximum height of the roughness	2.2μm
R_v	Maximum roughness valley depth	1.0μm
R_p	Maximum roughness peak height	1.2μm
R_{tm}	Average maximum height of the roughness	1.4μm
R_{vm}	Average maximum roughness valley depth	0.7μm
R_{pm}	Average maximum roughness peak height	0.7μm
R_{3z}	Average third height peak to third lowest valley height	1.9μm
$R_{3z\ ISO}$	Average third highest peak to third lowest valley height	1.1μm
R_z	Average maximum height of the profile	2.1μm
$R_{z\ ISO}$	Average maximum height of the roughness	1.4μm
R_{sk}	Skewness	0.010
R_{ku}	Kurtosis	2.862
W_a	Waviness average	249.9μm
W_q	Root mean square waviness	250.0μm
$W_y=W_{max}$	Waviness maximum height	261.9μm
P_t	Maximum height of the profile	262.7μm
Spatial		
Λ_a	Average wavelength of the profile	0.028mm
Λ_q	Root mean square (RMS) wavelength of the profile	16.462μm
Hybrid		
Δ_a	Average absolute slope	0.06931μm
Δ_q	Root mean square (RMS) slope	146.0×10^{-6}
l	Length	2.773mm
L_0	Developed profile length	2.784mm
L_r	Profile length ratio	1.016

(e)

Amplitude		
R_a	Roughness Average	0.23μm
R_q	Root mean square roughness	0.29μm
R_t	Maximum roughness value depth	1.16μm
R_v	Maximum roughness valley depth	0.83μm
R_p	Maximum roughness peak height	0.78μm
R_{tm}	Average maximum height of the roughness	1.05μm
R_{vm}	Average maximum roughness valley depth	0.52μm
R_{pm}	Average roughness peak height	0.53μm
R_{3z}	Average third height peak to third lowest valley height	1.32μm
$R_{3z\ ISO}$	Average third highest peak to third lowest valley height	0.71μm
R_z	Average maximum height of the profile	1.41μm
$R_{z\ ISO}$	Average maximum height of the roughness	1.05μm
R_{sk}	Skewness	-0.009
R_{ku}	Kurtosis	2.891
W_a	Waviness average	98.47μm
W_q	Root mean square waviness	98.49μm
$W_y=W_{max}$	Waviness maximum height	102.95μm
P_t	Maximum height of the profile	103.24mm
Spatial		
Λ_a	Average wavelength of the profile	0.027mm
Λ_q	Root mean square (RMS) wavelength of the profile	16.461μm
Hybrid		
Δ_a	Average absolute slope	0.05326μm
Δ_q	Root mean square (RMS) slope	110.0×10^{-6}
L	Length	1.805mm
L_0	Developed profile length	1.809mm
L_r	Profile length ratio	1.004

(c)

(f)

Fig. 3 **a–c** 3d profilometer images of the substrates without CVD diamond coatings. **d–f** 3d profilometer images of the MCD CVD diamond coatings

the indentation hardness is given by the indenter load divided by the projected area of contact. In order to calculate the indentation hardness, the displacement of the indenter (known geometry) is measured and the full load contact area is estimated from the contact depth ($h_c <$ penetration depth). A characteristic load–displacement curve of the nanoindentation test shows an elastic–plastic loading curve followed by an elastic unloading curve. Slope of this elastic unloading curve segment gives the elastic modulus of the material. Elastic modulus $(E) = $ (slope of the elastic unloading curve) $\times (\sqrt{/2\sqrt{}})$. Hardness $(H) = /$, where $P = $ maximum load and $A = $ area of contact. $h, = 3 (3h_c^2)^{1/2}\tan^2 65.27$, where h_c is the contact depth. The three-face Berkovich indenter is the most accepted choice of geometry for nanoindentation testing. Hardness of the polished MCD coatings was measured using a nanoindenter (TI 950, HYSITRON) fitted with a Berkovich tip of total included angle $(a) = 130.5°$ and the radius of curvature ~ 150 nm. Trapezoidal load cycle
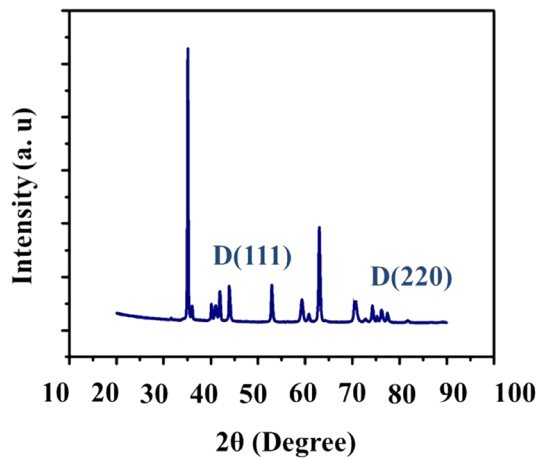
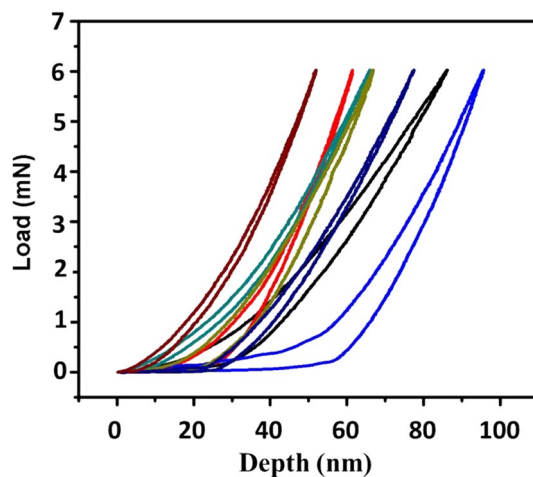**Fig. 4** XRD pattern for CVD diamond on titanium alloy

Fig. 5 Load–displacement curves corresponding to 7 indentations on MCD coating

(10 mN) was used, and the hardness and elastic modulus values were measured from the load displacement data using Oliver and Pharr method [29].

The thickness of the MCD coatings was ~ 3 μm. Figure 5 shows the load–displacement curves for the polished MCD coatings. Seven indentation tests were performed on each coating using nanoindentation technique. It was evident from the load–displacement curves that the MCD coatings were resistant to deformation. The average indentation depth for MCD coating was 65 nm. The average hardness of MCD coatings was found to be ~ 55 GPa, and these values are in agreement with the earlier reports on diamond films [30, 31].

Mechanical characteristics of the CVD diamond coatings are usually classified into interfacial adhesion and hardness. Hardness of the CVD diamond primarily depends up on its phase purity and crystallinity. Microstructural quality of

the adjacent interface materials and the type of bonding are responsible for adhesion between the coating and substrate. Adhesion between the CVD diamond and titanium alloy substrate is mainly by mechanical interlocking and hence depends on the (1) surface microstructure of the substrate (titanium alloy), which can be controlled by proper surface pre-treatment, and (2) quality of the diamond growth at the interface, which can be controlled by choosing the suitable process parameters to attain quality film growth. With the increase in non-diamond phases at the grain boundaries, the hardness of the CVD diamond coating decreases. High hardness is exhibited by phase pure and highly crystalline diamond. Inherently, CVD diamond coatings demonstrate exceptionally good tribological characteristics with high wear resistance and low friction coefficient. However, low friction coefficient values of about 0.05 can be achieved by reducing the crystallite size of the diamond to few nanometers.

Hardness is defined as the resistance to indentation and phase pure MCD coating is expected to show high hardness. Chowdhury et al. successfully applied the nanoindentation technique to measure the hardness and elastic modulus of the diamond coatings [32]. Catledge et al. demonstrated that the microstructured diamond coatings can be designed to get the hardness ranging from 10 GPa (medium hard) to 100 GPa (super-hard) which can be considered for a wide range of wear resistance applications [33]. Narayan et al. and Kulisch et al. used nanoindentation technique to measure the hardness of NCD coating (45.3 ± 14.6 GPa) and nanocrystalline diamond/amorphous carbon composite coating (39.7 ± 2.2 GPa), respectively [34, 35]. However, MCD coatings exhibit much higher hardness because of their high crystallinity.

3.6 Tribological Characteristics

Tribological characteristics for instance friction and wear between two contact surfaces are highly scale dependent. The origin of the friction and wear characteristics that is observed on the macroscopic level is found in the mechanisms that take place at the micro-level. The micro-tribology helps in understanding the interaction between the materials at asperity-to-asperity level and to study the third body or tribolayer formation. Also, the micro-tribological studies facilitate the understanding of the interfacial phenomena on a small scale and of microstructures. Tribological experiments at micro-level give reliable information on interaction between the sliding surfaces due to its multiple asperity contact configuration [36]. Micro-tribometer (CSM Instruments, Switzerland) attached with the reciprocating tribomodule was used to carry out the experiments. This reciprocating module reproduces the reciprocating motion of many real-world mechanisms and allows recording the friction coefficient during forward and backward movements. The normal

load can be varied from 1 to 10 N, and the linear speed can be varied from 2 to 12 cm/s. The total sliding distance value in meters can be set for each test. As the disk reciprocates, the resulting frictional forces acting between the ball and the disk are measured by very small deflections of the frictionless lever (ball holder) using a linear variable differential transformer (LVDT) sensor. Another LVDT sensor was coupled to the tribometer to measure the total contact wear depth during the test. The sliding tribological and wear characteristics of the diamond coatings were studied against alumina balls of size Ø6 mm under dry atmospheric test conditions, and wear track morphology was studied using Raman, EDS, SEM and HRSEM.

The graph of substrate is stable from the beginning of the test due to the polished surface, while stabilized linearity of MCD comes after a period of instability. A run-in period is required for as-deposited films to reach a low steady-state value, ascribed to the surface roughness and the average grain size, spawning the abrasive cutting and plowing effects to the sharp surface asperities. Conversely, wear rate is another significant performance indicator in the friction test. However, wear of the tested diamond films was too stumpy to be calculated. Due to plugging, micro-abrasion is possible; when the film has greater hardness and elastic modulus compared with the ball, the wear loss from the ball surface may be higher than from diamond film surface [37]. As a result, specimens coated with diamond film ostensibly present better tribological properties than uncoated substrates [38]. Primarily, the difference of the friction coefficient in films is dependent on their initial roughness. Generally, the higher the surface roughness is, the greater the friction and wear losses are [39]. Secondly, after running in, the MCD surface is almost atomically smooth, and the friction coefficient represents the pure adhesive friction component. An explanation for the low adhesive component is that the so-called dangling carbon bonds at the surface are terminated by hydrogen [40]. If the hydrogen atoms are detached from the surface, the friction of self-mated diamond increases. Conventional CVD MCD

contains small amounts of hydrogen (0.5%). This could be caused by spontaneous supply of hydrogen to the surface and thereby improved tribological properties [41]. Furthermore, low friction is directly related to the amorphization/graphitization of diamond near the sliding contact point [42, 43]. It is observed that it undergoes the transition from sp^3 to sp^2 resulting in an amorphous adlayer that depends on surface orientation and sliding direction, when diamond is polished. The structural phase transformation and amorphization influence the friction and wear performances. Enhanced amorphization/graphitization of carbon reduces the shear resistance and hence lowers the friction coefficient. Thus, the low friction coefficient in the final stabilized liner can be attributed to the formation of a continuous lubricating amorphous carbonaceous layer. On the other hand, the low friction character of diamond is largely attributed to the highly passive nature of its sliding surface. Active gaseous species such as water vapor can be adsorbed and passivate the dangling surface bonds of most carbon materials, which prohibit the formation of bond between specimens and counterparts. With the increase in load, the friction coefficient would decrease according to Kumar et al. [44]. As diamond undergoes plasticity induced amorphization/graphitization, the extent of phase transformation is expected to increase with the increase in applied load. More asperities would appear at high normal load, resulting in intimate contact between specimens and counterparts. As a consequence, the thickness of the transfer layer will increase and the COF will decrease. With the increase in film thickness, both grain size and roughness of MCD would increase simultaneously [45]. Comprehensively, all these characteristics of diamond films are beneficial to biological applications. For reducing friction, diamond-coated titanium alloy is better than titanium alloy itself. And MCD film is testified to be more advantageous than virgin titanium alloy since it gains a longer working life.

Figure 6a shows the friction curves of the uncoated substrates against alumina ball, while Fig. 6b shows the friction curves of the MCD coatings sliding against alumina ball that

Fig. 6 **a** Tribological characteristics of uncoated Ti6Al4V sliding against alumina ball. **b** Tribological characteristics of MCD coating sliding against alumina ball
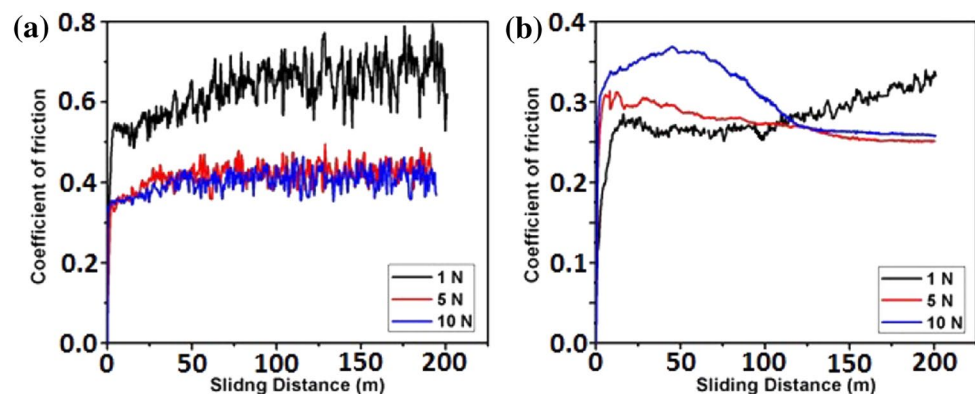
are plotted against sliding distance. Unstable friction behavior was observed during the sliding of MCD coating against alumina ball. Friction values of ~0.25–0.35, ~0.25–0.325 and ~0.24–0.375 were observed at 1, 5 and 10 N, respectively, with the MCD coating. The average values of coefficient of friction in case of MCD coatings are ~0.3, ~0.2875 and ~0.3075. The high run-in friction behavior of the MCD coating was attributed to its sharp and rough surface asperities. Friction values of ~0.55–0.8, ~0.36–0.43 and ~0.35–0.425 were observed in case of uncoated substrate at a load of 1, 5 and 10 N, respectively. The average values of the coefficient of friction in case of virgin substrate are 0.675, 0.395 and 0.3875. The detailed tribological experimental results are listed in Table 2.

CVD diamond coating performs exceedingly well under dry sliding conditions against itself and many other ceramic materials such as alumina, Si_3N_4, SiC due to the chemical inertness, high hardness and low friction coefficient. The tribological characteristics of CVD diamond coatings are dependent on the presence of non-diamond phases, grain size and their grain boundary strength [46]. Also, the wear and friction behavior of the tribocontact pairs during dry sliding depends on the extrinsic conditions such as sliding velocity, normal load and mainly on the type of interaction, whether chemical or mechanical [47]. The contact between two sliding surfaces occurs at asperities, and these asperities act as stress concentrators. CVD diamond coatings experience only mechanical wear by means of asperity fracture and abrasive damage and are highly wear resistant and chemically inert while sliding against most of the ceramics [48]. Due to the abrasive micro-wear mechanisms, grooves may form on the wear surfaces in sliding contact [49]. Purely mechanical wear generally shows stable friction behavior and produces rough contact surfaces, whereas the mating parts produce tribodebris or tribolayer at the contact interface and modify the contact stresses due to tribochemical interactions or tribooxidation [50]. These tribolayers of the reaction products affect the wear and friction properties, since they are generally softer than the substrate, especially under un-lubricated conditions [51, 52]. The counter face material plays an important role in determining the friction characteristics of diamond coatings. In the case of non-diamond sliders, the friction is influenced by the creation

of a transfer layer during run-in period. Bull et al. found that the initial friction between CVD diamond coating and sapphire was ~0.2, but raised quickly to ~0.6, which was attributed to the formation of thick transfer layer [53]. Diamond is regarded as self-lubricating material, and the low friction coefficient values achieved by many researchers are primarily due to its utmost chemical inertness (no chemical interaction/bonding) and sliding stimulated graphitization or re-hybridization of carbon. The chemistry of the sliding environment such as use of vacuum and relative humidity, inert gases or any other gases may affect the friction and wear characteristics of the diamond films [54, 55].

The wear and friction of diamond coatings are much higher in vacuum and at high temperatures, whereas it is normally low only in air and relatively dry inert gas environment [56, 57]. Gaseous adsorbates such as hydrogen or oxygen can effectively reduce the chemical reactivity of the free σ-bonds on the surface of diamond. The adhesion component of the friction significantly reduces when these σ-bonds become highly passive and such diamond surface exhibits low friction coefficient [58]. A high surface roughness of the faceted MCD coatings has a detrimental effect on the friction and wear characteristics [59]. However, due to the hard and sharp asperities these coatings hardly show any wear but severely abrade counter face materials [60]. Generally, MCD coatings exhibit high run-in friction behavior and stabilize to the lower value after a long sliding distance.

Only surface asperity level wear was observed on MCD coatings. Figure 7a, b shows the magnified wear track regions of the virgin substrate and MCD coatings. Micro-grooves were observed on the wear track of the MCD coatings.

4 Conclusion

1. MCD coatings have yielded a super-hardness of 55 GPa. The observed high hardness of the MCD coating was attributed to the absence of graphitic phases as shown by Raman spectroscopy.

2. The MCD coatings show an average coefficient of friction of ~0.3–0.287 when sliding against Al_2O_3 balls. An unstable coefficient of friction is observed in MCD coat-

Table 2 Friction values obtained during friction tests at three loads

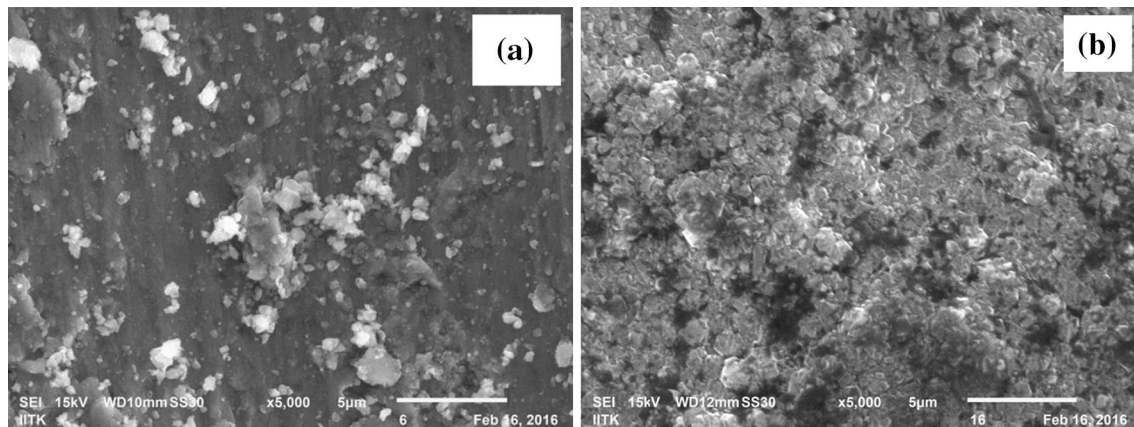| Material	Range of COF at 1 N	Range of COF at 5 N	Range of COF at 10 N	Average COF at 1 N	Average COF at 5 N	Average COF at 10 N
Ti6Al4V	0.55–0.8	0.36–0.43	0.35–0.425	0.675	0.395	0.387
MCD	0.25–0.35	0.25–0.325	0.24–0.375	0.3	0.287	0.307
Percentage reduction in average COF				55.5	27.21	20.6

Fig. 7 SEM images of wear track **a** Substrate without coatings. **b** MCD CVD diamond coatings

ings due to the surface roughness and surface asperities on the MCD coating surface.

3. The wear of the diamond coating is negligible. The alumina balls are worn out quickly as compared to the diamond coatings.

References

1. Amaral M, Maru MM, Rodrigues SP, Gouvêa CP, Trommer RM, Oliveira FJ, Achete CA, Silva RF (2015) Extremely low wear rates in hip joint bearings coated with nanocrystalline diamond. Tribol Int 89:72–77
2. Salar Elahi A, Ghoranneviss M (2015) Application of the HFCVD technique for growth of nano-rods and nano-crystals. J Cryst Growth 410:82–92
3. Spitsyn BV, Bouilov LL, Derjaguin BV (1981) Vapor growth of diamond on diamond and other surfaces. J Cryst Growth 52:219–226
4. Angus JC, Argoitia A, Gat R, Li Z, Sunkara M, Wang L, Wang Y (1993) Chemical vapour deposition of diamond. Philos Trans R Soc Lond Ser A Phys Eng Sci 342:195–208
5. DeVries RC (1987) Synthesis of diamond under metastable conditions. Annu Rev Mater Sci 17:161–187
6. Jones AC, Hitchman ML (2009) Chemical vapor deposition, precursors, processes and applications. RCS Publications
7. TaoZhang XL, Sun F, Zhang Z (2015) The deposition parameters in the synthesis of CVD microcrystalline diamond powders optimized by the orthogonal experiment. J Cryst Growth 426:15–24
8. Zhang CZ, Niakan H, Yang L, Li YS, Hu YF, Yang Q (2013) Study of diamond nucleation and growth on Ti6Al4V with tungsten interlayer. Surf Coat Technol 237:248–254
9. Miyoshi K (1996) Friction and wear properties of as-deposited and carbon ion-implanted diamond films. Mater Sci Eng A 209:38–53
10. Wang J, Zhoub J, Long HY, Xie YN, Zhang XW, Luo H, Deng ZJ, Wei Q, Yu ZM, Zhang J, Tang ZG (2014) Tribological, anti-corrosive properties and biocompatibility of the micro-and nano-crystalline diamond coated Ti6Al4V. Surf Coat Technol 258:1032–1038
11. Schafer L, Hofer M, Kroger R (2006) The versatility of hot-filament activated chemical vapor deposition. Thin Solid Films 515:1017–1024
12. Liu MN, Bian YB, Zheng SJ, Zhua T, Chena YG, Chenb YL, Wang JS (2015) Growth and mechanical properties of diamond films on cemented carbide with buffer layers. Thin Solid Films 584:165–169
13. May PW, Smith JA, Mankelevich Y (2006) Deposition of NCD films using hot filament CVD and Ar/CH$_4$/H$_2$ gas mixtures. Diam Relat Mater 15:345–352
14. Tsai H-Y, Tseng P-T (2015) Field emission characteristics of diamond nano-tip array fabricated by anodic aluminum oxide template with nano-conical holes. Appl Surf Sci 351:1004–1010
15. Chen N, Pua L, Sunb F, He P, Zhua Q, Ren J (2015) Tribological behavior of HFCVD multilayer diamond film on silicon carbide. Surf Coat Technol 272:66–71
16. Long H, Lia S, Luo H, Wang Y, Wei P, Yu ZM (2015) The effect of periodic magnetic field on the fabrication and field emission properties of nanocrystalline diamond films. Appl Surf Sci 353:548–552
17. Sarangi SK, Chattopadhyay A, Chattopadhyay AK (2012) Influence of process parameters on growth of diamond crystal on cemented carbide substrates by HFCVD system. Int J Refract Met Hard Mater 31:1–13
18. Liang Q, Stanishevsky A, Vohra YK (2008) Tribological properties of undoped and boron-doped nanocrystalline diamond films. Thin Solid Films 517:800–804
19. Ali M, Urgen M (2011) Surface morphology, growth rate and quality of diamond films synthesized in hot filament CVD system under various methane concentrations. Appl Surf Sci 257:8420–8426
20. Trava-Airoldi VJ, Corat EJ, Peiia AFV, Leite NF, Baranauskas V, Salvadori MC (1995) Columnar CVD diamond growth structure on irregular surface substrates. Diam Relat Mater 4:1255–1259
21. Jeon ID, Park CJ, Kim DY, Hwang NM (2001) Effect of methane concentration on size of charged clusters in the hot filament diamond CVD process. J Cryst Growth 223:6–14
22. Williams OA, Daenen M, D'Haen J, Haenen K, Maes J, Moshchalkov VV, Nesládek M, Gruen DM (2006) Comparison of

the growth and properties of ultrananocrystalline diamond and nanocrystalline diamond. Diam Relat Mater 15:654–658

23. Buijnsters JG, Vázquez L, ter Meulen JJ (2009) Substrate pretreatment by ultrasonication with diamond powder mixtures for nucleation enhancement in diamond film growth. Diam Relat Mater 18:1239–1246

24. Sumant AV, Grierson DS, Gerbi JE, Carlisle JA, Auciello O, Carpick RW (2007) Surface chemistry and bonding configuration of ultrananocrystalline diamond surfaces and their effects on nanotribological properties. Phys Rev B 76:235429

25. Amaral M, Silva DJ, Fernandes AJS, Costa FM, Oliveira FJ, Silva RF (2009) Surface activation pre-treatments for NCD films grown by HFCVD. Vacuum 83:1228–1232

26. Miyoshi K, Wu RLC (2001) Measurements and diagnostics of diamond films and coatings. Measurement 29:113–126

27. Knight DS, White WB (1989) Characterization of diamond films by Raman spectroscopy. J Mater Res 4:385–393

28. Gruen DM (1999) Nanocrystalline diamond films. Annu Rev Mater Sci 29:211–259

29. Oliver WC, Pharr GM (1992) An improved technique for determining hardness and elastic modulus using load and displacement sensing indentation experiments. J Mater Res 7:1564–1583

30. Wiora M, Brühne K, Flöter A, Gluche P, Willey TM, Kucheyev SO, Van Buuren AW, Hamza AV, Biener J, Fecht HJ (2009) Grain size dependent mechanical properties of nanocrystalline diamond films grown by hot-filament CVD. Diam Relat Mater 18:927–930

31. Michler J, Mermoux M, von Kaenel Y, Haouni A, Lucazeau G, Blank E (1999) Residual stress in diamond films: origins and modelling. Thin Solid Films 357:189–201

32. Chowdhury S, De Barra E, Laugier T (2004) Study of mechanical properties of CVD diamond on SiC substrates. Diam Relat Mater 13:1625–1631

33. Catledge SA, Borham J, Vohra YK, Lacefield WR, Lemons JE (2002) Nanoindentation hardness and adhesion investigations of vapor deposited nanostructured diamond films. J Appl Phys 91:5347–5352

34. Narayan RJ, Wei W, Jin C, Andara M, Agarwal A, Gerhardt RA, Shih CC, Shih CM, Lin SJ, Su YY, Ramamurti R, Singh RN (2006) Microstructural and biological properties of nanocrystalline diamond coatings. Diam Relat Mater 15:1935–1940

35. Kulisch W, Popov C, Boycheva S, Buforn L, Favaro G, Conte N (2004) Mechanical properties of nanocrystalline diamond/amorphous carbon composite films prepared by microwave plasma chemical vapour deposition. Diam Relat Mater 13:1997–2002

36. Achanta S, Liskiewicz T, Drees D, Celis JP (2009) Friction mechanisms at the micro-scale. Tribol Int 42:1792–1799

37. Panda K, Kumar N, Panigrahi B, Polaki S, Sundaravel B, Dash S, Tyagi A, Lin I-N (2013) Tribological properties of N+ ion implanted ultrananocrystalline diamond films. Tribol Int 57:124–136

38. Kulesza S, Patyk J, Rozpłoch F (2004) Spontaneous decrease of high surface electrical conductivity in diamond exposed to atmospheric air. Chem Phys Lett 391:56–59

39. Erdemir A, Bindal C, Fenske G, Zuiker C, Krauss A, Gruen D (1996) Friction and wear properties of smooth diamond films grown in fullerene+ argon plasmas. Diam Relat Mater 5:923–931

40. Pepper SV (1982) Effect of electronic structure of the diamond surface on the strength of the diamond–metal interface. J Vac Sci Technol 20:643–646

41. Hollman P, Wänstrand O, Hogmark S (1998) Friction properties of smooth nanocrystalline diamond coatings. Diam Relat Mater 7:1471–1477

42. Pastewka L, Moser S, Gumbsch P, Moseler M (2011) Anisotropic mechanical amorphization drives wear in diamond. Nat Mater 10:34–38

43. Grierson DS, Carpick RW (2007) Nanotribology of carbon-based materials. Nano Today 2:12–21

44. Kumar N, Panda K, Dash S, Popov C, Reithmaier J, Panigrahi B, Tyagi A, Raj B (2012) Tribological properties of nanocrystalline diamond films deposited by hot filament chemical vapor deposition. AIP Adv 2:032164

45. Wiora M, Brühne K, Flöter A, Gluche P, Willey T, Kucheyev S, Van Buuren A, Hamza A, Biener J, Fecht H-J (2009) Grain size dependent mechanical properties of nanocrystalline diamond films grown by hot-filament CVD. Diam Relat Mater 18:927–930

46. Bull SJ, Mathews A (1992) Diamond for wear and corrosion applications. Diam Relat Mater 1:1049–1064

47. Muratov VA, Luangvaranunt T, Fischer TE (1998) The tribochemistry of silicon nitride: effects of friction, temperature and sliding velocity. Tribol Int 31:601–611

48. Bull SJ (1995) Tribology of carbon coatings: DLC, diamond and beyond. Diam Relat Mater 4:827–836

49. Kato K (1992) Micro-mechanisms of wear–wear modes. Wear 153:277–295

50. Blomberg A, Hogmark S, Lu J (1993) An electron microscopy study of worn ceramic surfaces. Tribol Int 26:369–381

51. Fischer TE, Tomizawa E (1985) Interaction of tribochemistry and microfracture in the friction and wear of silicon nitride. Wear 105:29–45

52. Fischer TE (1988) Tribochemistry. Annu Rev Mater Sci 18:303–323

53. Bull SJ, Chalker PR, Johnston C, Moore V (1994) The effect of roughness on the friction and wear of diamond thin films. Surf Coat Technol 68–69:603–610

54. Erdemir A, Halter M, Fenske GR, Zuiker C, Csencsits R, Krauss AR, Gruen DM (1997) Friction and wear mechanisms of smooth diamond films during sliding in air and dry nitrogen. Tribol Trans 40:667–675

55. Kumar N, Radhika R, Kozakov AT, Sankaran KJ, Dash S, Tyagi AK, Tai NH, Lin N (2013) Humidity-dependent friction mechanism in an ultrananocrystalline diamond film. Appl Phys 46:275501

56. Chandrasekar S, Bhushan B (1992) The role of environment in the friction of diamond for magnetic recording head applications. Wear 153:79–89

57. Miyoshi K, Wu RLC, Garscadden A, Barnes PN, Jackson HE (1993) Friction and wear of plasma-deposited diamond films. J Appl Phys 74:4446–4454

58. Erdemir A (2002) Friction and wear of diamond and diamond-like carbon films. J Eng Tribol 216:387–400

59. Miki H, Tsutsui A, Takeno T, Takagi T (2012) Friction properties of partially polished CVD diamond films at different sliding speeds. Diam Relat Mater 24:167–170

60. Hayward IP, Singer IL, Seitzman LE (1992) Effect of roughness on the friction of diamond on CVD diamond coatings. Wear 157:215–227